An unsteady double diffusive natural convection in an inclined rectangular enclosure with different angles of magnetic field

*Sabyasachi Mondal and Precious Sibanda[†]

School of Mathematics, Statistics and Computer Science

University of KwaZulu-Natal

Pietermaritzburg-3209, Private Bag X01, Scottsville, South Africa

* Corresponding author: sabya.mondal.2007@gmail.com

† sibandap@ukzn.ac.za

An unsteady double-diffusive natural convection flow in an inclined rectangular enclosure subject to an applied magnetic field and heat generation parameter. The enclosure is heated and concentrated from one side and cooled from the adjacent side. The other two sides are adiabatic. The governing equations have been solved numerically using a staggered grid finite-difference method to determine the streamline, isotherm and iso-concentration patterns. We have further obtained the local and average Nusselt numbers and local and average Sherwood numbers for various values of buyancy ratio and angles of the magnetic field by considering three different inclination angles of the enclosure while keeping the aspect ratio fixed. The results indicate that the flow pattern, temperature and concentration fields are significantly dependent on the thermal radiation and the magnetic field angles. It is found that different angles of the magnetic field suppress the convection flow and its direction influences the flow pattern. This leads to the appearance of inner loop and multiple eddies.

Keywords: Double- diffusive natural convection; Inclined rectangular cavity; Magnetic field angles; Buoyancy ratio.

1. Introduction

The study of magnetic field effect and buyancy ratio on double diffusive natural convection in a fluid-saturated cavity have received considerable attention in recent years due to its wide variety of applications in engineering and technology processes such as solar energy collection, nuclear reactor insulation, cooling of electronic devices, furnaces, drying technologies and crystal growth in liquids, etc. As the Lorentz force suppresses the convection currents by reducing the velocities when the fluid is electrically conducting and exposed to a magnetic field, a external magnetic field is used as a flow control mechanism in manufacturing industries. Rudraiah et al. (1995) studied the effect of a magnetic field on free convection inside a rectangular enclosure. They found that a circular flow was formed with a relatively weak magnetic field, the convection was suppressed and the rate of convective heat transfer decreased when the magnetic field strength was increased. Garandet et al. (1992) analyzed the effect of magnetic field on buoyancy driven convection in a rectangular enclosure. Sarris et al. (2005) examined two-dimensional unsteady simulations of MHD natural convection of a liquid-metal in a laterally and volumetrically heated square cavity. Mansour et al. (2010) studied the effects of an inclined magnetic field on the unsteady natural convection in an inclined cavity filled with a fluid saturated porous medium considering heat source in the solid phase. Al-Najem et al. (1998) showed that an increase in the Hartmann number causes reduction in the heat transfer rate from cavity sidewalls. Ece and Büyük (2006) found solutions for the velocity and temperature fields inside the rectangular enclosure and determined the effect of the strength and direction of the magnetic

field, the aspect ratio and the inclination of the enclosure on the transport phenomena. Later, Ece and Büyük (2007) investigated the steady natural convection flow in an inclined square enclosure with differentially heated adjacent walls under the influence of magnetic field. Jordan (2007) studied the effects of thermal radiation and viscous dissipation on MHD unsteady free-convection flow over a semi-infinite vertical porous plate. He examined the velocity, temperature, local skin-friction and local Nusselt number for various physical parameters like the Eckert number, magnetic number and suction (or injection). The effect of heat-generation/absorbtion in an enclosure in the presence of magnetic field also plays an important role in convective flows. Grosan et al. (2009) discussed the effects of magnetic field and internal heat generation on the free convection in a rectangular cavity filled with a porous medium. Thereafter, Mahapatra et al. (2013) numerically examined the effects of buoyancy ratio and thermal Rayleigh number on double diffusive natural convection in a cavity when boundaries are uniformly and non-uniformly heated and concentrated. Rahman and Sharif (2003) investigated the laminar natural convection in differentially heated inclined rectangular enclosures of various aspect ratios. Chamkha and Al-Naser (2001) considered laminar double-diffusive convective flow of a binary gas mixture in an inclined rectangular enclosure filled with a uniform porous medium. A numerical investigation of double-diffusive laminar mixed convection in an inclined cavity has been studied by Teamah et al. (2011). Wang et al. (2008) studied the natural convection heat transfer in an inclined porous cavity with time-periodic boundary conditions numerically. Teamah et al. (2013) studied doublediffusive convective flow in an inclined rectangular enclosure with the shortest sides being insulated and impermeable. On the other hand, studies on the combination of radiative heat transfer and heat generation with convection or conduction were intensified because the effect of the radiation heat transfer and heat generation is more important, particularly in the presence of a participating medium and / or radiative surfaces with large emissivities [Mahapatra et al. (2012; 2011)]. Recent developments in hypersonic flights, missile reentry rocket combustion chambers and gas cooled nuclear reactors have focused attention of researchers on thermal radiation, heat generation and emphasize the need for inclusion of heat transfer in these processes. Moufekkir et al. (2013) investigated double- diffusive natural convection and radiation in an inclined cavity using lattice Boltzmann method. After that, Mahapatra et al. (2013) studied mixed convection flow in an inclined enclosure under magnetic field with thermal radiation and heat generation. They had studied the radiation and heat generation effects in a inclined cavity with different magnetic field angle. Recently, Mondal and Sibanda (2015) studied studied effects of buoyancy ratio on unsteady double-diffusive natural convection in a cavity filled with porous medium with non-uniform boundary conditions. Not much attention has been given to the study of the effects of the buoyancy ratio on double diffusive natural convection flow when the magnetic field acts at different angles in an inclined rectangular enclosure with heat generation and uniform boundary conditions (i.e. the rectangular enclosure is heated and concentrated from the left vertical wall and cooled from the top wall by keeping other walls in adiabatic state). The present study deals with the effects of the buoyancy ratio on unsteady double-diffusive natural convection in an inclined rectangular enclosure with different angle of magnetic field in presence of heat generation parameter. The streamline pattern, isotherms, iso-concentrations, average Nusselt number and average Sherwood number are presented graphically and in tabular forms.

2. Governing equations and boundary conditions

An unsteady-state flow in two-dimensional rectangular cavity of height H and length is L as shown in Fig.1 is considered. The thermophysical properties of the fluid are assumed

Double diffusive natural convection in an inclined rectangular enclosure 3

to be constant except the density variation in the buoyancy force, which is approximated according to the Boussinesq approximation. This variation, due to both temperature and concentration gradients, can be described by the following equation:

$$\rho = \rho_0 [1 - \beta_T (T - T_c) - \beta_C (C - C_c)], \tag{1}$$

where β_T and β_C are the thermal and concentration expansion coefficients, respectively. The angle of inclination of the enclosure with the horizontal line in the counter-clockwise

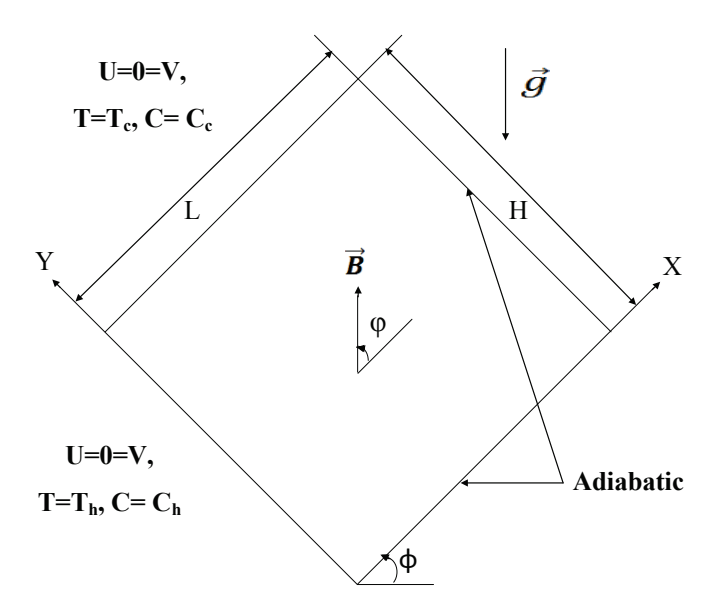


Fig. 1. Geometry and the coordinate system.

direction is denoted by ϕ . The magnetic field strength B_0 is applied at an angle φ with respect to the coordinate system. The right and the bottom walls are insulated and the fluid is isothermally heated and cooled at the left and top walls with uniform temperature of T_h and T_c , respectively. The magnetic Reynolds number is assumed to be small and the induced magnetic field due to the motion of the electrically conducting fluid is neglected [Shercliff (1965)]. The Joule heating of the fluid and the effect of viscous dissipation are also negligible.

The governing equations under Boussinesq approximation are written as:

$$\frac{\partial U}{\partial X} + \frac{\partial V}{\partial Y} = 0, \tag{2}$$

$$\rho_0 \frac{\partial U}{\partial t'} + \rho_0 \left(U \frac{\partial U}{\partial X} + V \frac{\partial U}{\partial Y} \right) = -\rho_0 [1 - \beta_T (T - T_C) - \beta_S (C - C_c)] g \sin \phi$$

$$- \frac{\partial P}{\partial X} + \mu \left(\frac{\partial^2 U}{\partial X^2} + \frac{\partial^2 U}{\partial Y^2} \right) + \sigma B^2 (V \sin \varphi \cos \varphi - U \sin^2 \varphi), \tag{3}$$

$$\rho_0 \frac{\partial V}{\partial t'} + \rho_0 \left(U \frac{\partial V}{\partial X} + V \frac{\partial V}{\partial Y} \right) = -\rho_0 [1 - \beta_T (T - T_c) - \beta_S (C - C_c)] g \cos \phi$$

$$- \frac{\partial P}{\partial Y} + \mu \left(\frac{\partial^2 V}{\partial X^2} + \frac{\partial^2 V}{\partial Y^2} \right) + \sigma B^2 (U \cos \varphi \sin \varphi - V \cos^2 \varphi), \tag{4}$$

$$\frac{\partial T}{\partial t'} + U \frac{\partial T}{\partial X} + V \frac{\partial T}{\partial Y} = \alpha \left(\frac{\partial^2 T}{\partial X^2} + \frac{\partial^2 T}{\partial Y^2} \right) + \frac{Q}{\rho_0 C_p} (T - T_c), \tag{5}$$

$$\frac{\partial C}{\partial t'} + U \frac{\partial C}{\partial X} + V \frac{\partial C}{\partial Y} = D \left(\frac{\partial^2 C}{\partial X^2} + \frac{\partial^2 C}{\partial Y^2} \right). \tag{6}$$

The associated boundary conditions are

$$U(X,0) = U(X,H) = U(0,Y) = U(L,Y) = 0,$$
(7)

$$V(X,0) = V(X,H) = V(0,Y) = V(L,Y) = 0,$$
(8)

$$T(0,Y) = T_h, T(X,H) = T_c, \frac{\partial T}{\partial X}(L,Y) = \frac{\partial T}{\partial Y}(X,0) = 0,$$
(9)

$$C(0,Y) = C_h, C(X,H) = C_c, \frac{\partial C}{\partial X}(L,Y) = \frac{\partial C}{\partial Y}(X,0) = 0.$$
(10)

Dimensionless variables used in the analysis are defined as,

$$t = \frac{\alpha t'}{LH}, x = \frac{X}{L}, \quad y = \frac{Y}{H}, \quad \delta = \frac{H}{L}, \quad u = \frac{HU}{\alpha}, \quad v = \frac{LV}{\alpha}, \tag{11}$$

$$\theta = \frac{T - T_c}{T_h - T_c}, \quad S = \frac{C - C_c}{C_h - C_c}, \quad p = \frac{[P + \rho_0 g(X \sin\phi + Y \cos\phi)] L^2}{\rho_0 \alpha^2}.$$
 (12)

where, X and Y are the distances measured along the horizontal and vertical directions respectively; U and V are velocity components in the X- and Y- directions respectively; T and C denote the temperature and concentration respectively; ν , α and D are kinematic viscosity, thermal diffusivity and mass diffusivity respectively; μ is viscosity; P is the pressure and ρ is the density; T_h and T_c are the temperatures at the hot and cold walls respectively; C_h and C_c are the concentrations at the hot and cold walls respectively; C_p and Q are specific heat at constant pressure and heat generation parameter.

The dimensionless governing equations are as follows:

$$\frac{\partial u}{\partial x} + \frac{\partial v}{\partial y} = 0, (13)$$

$$\frac{\partial u}{\partial t} = -\frac{\partial p}{\partial x} + P_r \left(\frac{1}{\delta} \frac{\partial^2 u}{\partial x^2} + \frac{1}{\delta^3} \frac{\partial^2 u}{\partial y^2} \right) - \frac{1}{\delta^2} \left(\frac{\partial u^2}{\partial x} + \frac{\partial uv}{\partial y} \right) + Gr_T P_r^2 (\theta + NS) \sin \phi$$

$$+Ha^2P_r(v\sin\varphi\cos\varphi - \frac{1}{\delta}u\sin^2\varphi),$$
 (14)

$$\frac{\partial v}{\partial t} = -\frac{\partial p}{\partial u} + P_r \left(\delta \frac{\partial^2 u}{\partial x^2} + \frac{1}{\delta} \frac{\partial^2 u}{\partial u^2} \right) - \left(\frac{\partial v^2}{\partial u} + \frac{\partial uv}{\partial x} \right) + \delta Gr_T P_r^2 (\theta + NS) \cos \phi$$

$$+Ha^{2}P_{r}(u\cos\varphi\sin\varphi-\delta v\cos^{2}\varphi),\tag{15}$$

$$\frac{\partial \theta}{\partial t} = \left(\delta \frac{\partial^2 \theta}{\partial x^2} + \frac{1}{\delta} \frac{\partial^2 \theta}{\partial y^2}\right) - \left(\frac{\partial u \theta}{\partial x} + \frac{\partial v \theta}{\partial y}\right) + \delta H e \ \theta. \tag{16}$$

$$\frac{\partial S}{\partial t} = \frac{1}{Le} \left(\delta \frac{\partial^2 S}{\partial x^2} + \frac{1}{\delta} \frac{\partial^2 S}{\partial y^2} \right) - \left(\frac{\partial uS}{\partial x} + \frac{\partial vS}{\partial y} \right). \tag{17}$$

Here, dimensionless parameters are

$$Gr_T = g\beta_T(T_h - T_c)L^3/\nu^2, Gr_C = g\beta_S(C_h - C_c)L^3/\nu^2, Ha = LB_0\sqrt{\frac{\sigma^*}{\mu}}$$
 (18)

$$P_r = \frac{\mu}{\rho_0 \alpha}, N = \frac{Gr_C}{Gr_T}, Ra = Gr_T Pr, He = \frac{QL^2}{k}.$$
 (19)

Dimensionless boundary conditions are

$$u = 0, \quad v = 0 \text{ on } x = 0, 1 \text{ and } y = 0, 1.$$
 (20)

$$\theta = 1$$
 on $x = 0$ and $\theta = 0$ on $y = 1$. (21)

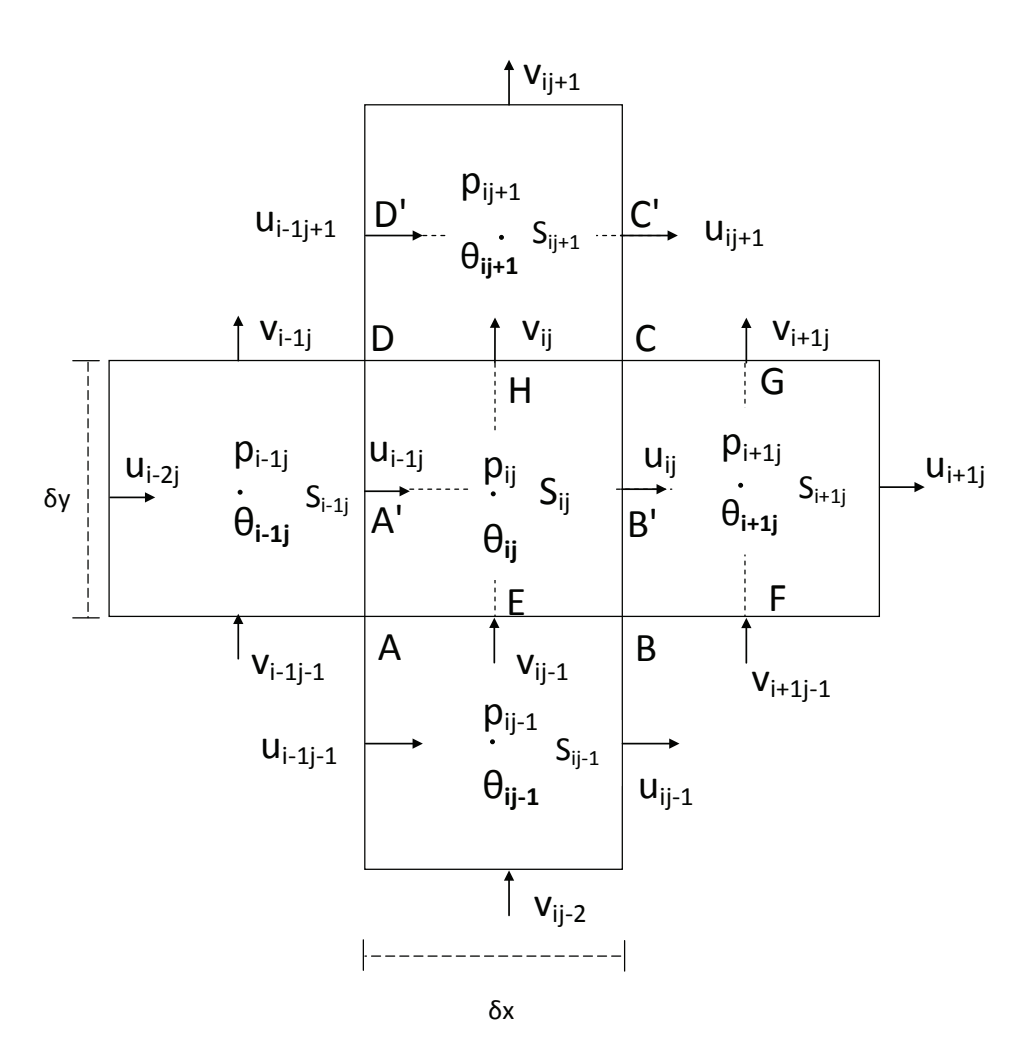
$$(\partial \theta / \partial x) \Big|_{x=1} = 0 \text{ and } (\partial \theta / \partial y) \Big|_{y=0} = 0.$$
 (22)

$$S = 1$$
 on $x = 0$ and $S = 0$ on $y = 1$. (23)

$$(\partial S/\partial x)\Big|_{x=1} = 0$$
 and $(\partial S/\partial y)\Big|_{y=0} = 0.$ (24)

Here, δ , N, Le, Pr, Gr_C , Gr_T , σ^* and He are aspect ratio of the enclosure, buoyancy ratio, Lewis number, Prandtl number, solutal Grashof number, thermal Grashof number, Stefan-Boltzmann constant and heat generation parameter respectively.

$$Nu$$
 and \overline{Nu}_H are defined by,
 $Nu = -\delta \frac{\partial \theta}{\partial x} \Big|_{x=0}$ and $\overline{Nu}_H = \delta \int_0^1 Nu \ dy$.



 $\mbox{Fig. 2. Control volume for u-momentum, v-momentum, temperature and concentration equations. } \\$

2.1. Solution procedure and numerical stability criteria

A control-volume based finite-difference discretization of the continuity, momentum, temperature and concentration equations is carried out using a staggered grid, popularly known as MAC cell method. The velocity components u and v are evaluated at different locations in the control volume whereas the pressure, temperature and concentration are

evaluated at the same location of the control volume as shown in Fig. 2. We note from Fig. 2 that the velocity components u, v are stored at the mid point of the vertical and horizontal faces respectively whereas the pressure, temperature and concentration values are stored at the centre of the cells. In the MAC method we use different cells to discretize different equations. For discretizing the continuity, temperature and concentration equations, we use the cell ABCD in Fig. 2.

Now the iteration process is described to obtain the solutions of the basic equations with appropriate boundary conditions. In the derivation of pressure-Poisson equation, the divergence term at n-th time level $(D_{i,j}^n)$ is retained and evaluated in the pressure-Poisson iteration. It is done because the discretized form of divergence of velocity field, i.e, D_{ij}^n is not guaranteed to be zero initially. The solution procedure starts with the initializing the velocity field. This is done either from the result of previous cycle or from the prescribed initial and boundary conditions. Using this velocity field pressure-Poisson equation is solved using Bi-CG-Stab method. Knowing the pressure field, equation for u-momentum, v-momentum, temperature and concentration are updated to get u, v, θ and S at (n+1)th time level. Then using the values of u and v at (n+1)th time level, the value of the divergence of velocity field is obtained and checked for its limit. If its absolute value is less than 0.5×10^{-5} and steady state is reached then iteration process stops, otherwise pressure-Poisson equation is solved again for pressure.

Linear stability of fluid flow gives $\delta t_1 \leq Min\left[\frac{\delta x}{|u|}, \frac{\delta y}{|v|}\right]$, which is related to the convection of fluid, i.e., fluid should not move more than one cell width per time step (Courant, Friedrichs and Lewy condition). Also, from the Hirt's stability analysis, we have $\delta t_2 \leq Min \left[\frac{1}{2Pr} \cdot \frac{\delta x^2 \cdot \delta y^2}{(\delta x^2 + \delta y^2)} \right]$. This condition roughly stated that momentum cannot diffuse more than one cell width per time step. The time step is determined from $\delta t = FCT \times [Min(\delta t_1, \delta t_2)],$ where the factor FCT varies from 0.2 to 0.4. The upwinding parameter β is governed by the inequality condition $1 \geq \beta \geq Max \left[\left| \frac{u\delta t}{\delta x} \right|, \left| \frac{v\delta t}{\delta y} \right| \right]$. As a rule of thumb, β is taken approximately 1.2 times larger than what is found from the above inequality condition.

3. Results and discussions

The working fluid in this study was chosen to be air with Prandtl number $P_r = 0.7$, heat generation parameter He = 1.0, Hartmann number $Ha = 10^2$, Lewis number Le = 1.0, Grashof number $Gr_T = 10^4$ and aspect ratio $\delta = 2$. The inclination angle ϕ of the enclosure, magnetic field angle φ in the enclosure and buoyancy ratio are such that $45^{\circ} \leq \phi \leq 135^{\circ}$, $45^{\circ} \leq \varphi \leq 135^{\circ}$ and $-20 \leq N \leq 20$ respectively.

Numerical results for the streamline, isotherm and iso-concentration contours inside the inclined rectangular cavity, average Nusselt and average Sherwood numbers distribution at the uniformly heated and concentrated surface of the inclined cavity for various values of the angle of magnetic field (φ) , buoyancy ratio (N) and inclination angle (ϕ) have been examined and are presented graphically in Figures 3 - 8 and in tabular form in Tables 1 - 3.

In order to obtain a grid independent solution to the problem, a grid refinement study is performed in Table 1 for $P_r = 0.7$, $Gr_T = 10^4$, $Ha = 10^2$, $\delta = 2$, Le = 1.0, N = 1.0, $He = 1.0, \varphi = 45^{\circ}, \phi = 45^{\circ}$ and N = 1. It is important to note that as the number of grid points are increased the value of $|\psi_{max}|$ increases. But when the number of grid points increases from 80×80 to 160×160 , no significant change is found in the value of $|\psi_{max}|$. Hence, all the results are computed taking 80×80 grid points.

A comparison of the average Nusselt number at the hot wall in absence of concentration

equation, thermal radiation parameter and heat generation parameter with same boundary conditions and same values of all other parameters are made with [Mahapatra et al. (2013); Ece and Büyük (2006)] for various values of ϕ and φ in Table 2. It is noted from this table that a very good agreement has been obtained with the previously published results.

Table 3 shows the average Nusselt numbers and sherwood numbers for different values of magnetic field angle φ , inclination angle of the cavity ϕ and buoyancy ratio N when the other parameters are fixed. It is seen from this table that when φ is fixed and N=20, the $\overline{Nu_H}$ is increases with increase in ϕ . But $\overline{Sh_H}$ decreases from $\phi=45^\circ$ to $\phi=90^\circ$ and afterthat opposite trend is observed. But when φ is fixed and N=1, both $\overline{Nu_H}$ and $\overline{Sh_H}$ are increase with increase in ϕ . Again, when φ is fixed and N=-20, both the $\overline{Nu_H}$ and $\overline{Sh_H}$ are decrease form $\phi=45^\circ$ to $\phi=90^\circ$ and after that the opposite trends are observed. For any value of N both the $\overline{Nu_H}$ and $\overline{Sh_H}$ are increased form $\phi=45^\circ$ to $\phi=90^\circ$ and afterthat the opposite trends are observed when ϕ is fixed. Again this table shows that if φ and φ are fixed then the $\overline{Nu_H}$ and $\overline{Sh_H}$ are decreased from N=20 to N=1 and after that opposite trends are observed (i.e., from N=1 to N=-20).

The numerical results for streamline, isotherm, iso-concentration contours are presented in Figures 3 - 8 for uniformly heated and concentrated walls for different values of φ , ϕ and N. The relative importance of thermal and solutal buoyancy forces is denoted by the buoyancy ratio (N) and is defined as the ratio of the solutal buoyancy force to thermal buoyancy force. This parameter is varied through a wide range -20 < N < 20; covering the concentration-dominated opposing flow (N = -20), pure thermal convection dominated flow (N=0), and concentration-dominated aiding flow (N=20). When N is sufficiently small i.e, the mass buoyancy is greater than the thermal buoyancy, the buoyancy forces that drive the fluid motion are mainly due to the gradients of temperature. Negative values of Nrepresent the opposing nature of two buoyancy forces, due to the negative coefficient of concentration expansion. In this limit, the so-called heat transfer driven flows, the distribution of constituent does not influence the flow pattern and the heat transfer rate. When N=1, the flow is steady; this is because in this case, the two buoyancies are equal to and oppose each other. When N > 1, the flows driven by buoyancy due to solutal gradients where the flow are mainly due to gradients of solute concentration. Clockwise and anticlockwise flows are shown via negative and positive signs of stream functions, respectively.

Fig. 3 shows the effect of N on the streamlines, isotherms and as well as on the isoconcentrations for wide range of variations in the buoyancy ratio (N) with uniformly heated and concentrated wall when $\varphi = 90^{\circ}$ and $\phi = 45^{\circ}$ for $P_r = 0.7$, $Gr_T = 10^4$, $Ha = 10^2$, $\delta = 2$, Le = 1.0 and He = 1.0. When N = 20 the streamlines are concentrated near the hot wall. Again when N = 1, as expected due to the cold fluids rise up from middle portion of the bottom wall and flow down along the two vertical walls forming two symmetric rolls with clockwise and anti-clockwise rotations inside the cavity. But, when N = -20 the streamlines are covered whole cavity with forming two eddies in the centre of the cavity in anticlockwise directions and the value of stream functions increases from the value of the stream functions when N = 1 due to the the strong circulations of fluid. In this figure we can see the isotherms are spreaded whole cavity when N = 20 but when N decreases the isotherms are concentrated near the cold wall. As the value of N more decreases the isotherms are more concentrated near the cold wall. The stronger circulation causes the temperature contours to be concentrated near the cold wall which may result in greater heat transfer rate due to convection. Again, in this figure we can see that iso-concentration contours are concentrated

near edge of the hot wall and cold wall in one side and the edge of hot wall and adiabatic wall on the other side. But, as the value of N decreases from 20 to -20 the iso-concentration contours of the one side of the cavity are dispersed towards the adiabatic wall this is due to higher mass transfer rate.

Streamline, isotherm and iso-concentration contours for different values of N when $P_r =$ $0.7, Gr_T = 10^4, Ha = 10^2, \delta = 2, Le = 1.0, He = 1.0, \varphi = 90^\circ \text{ and } \phi = 90^\circ \text{ with }$ uniformly heated and concentrated wall are displayed in Fig. 4. As the inclination angle increases the streamlines forms a single eddy near the uniformly heated and concentration wall with anticlockwise directions when N=20. The center of the single eddy is slightly shifted away from the heated wall towards the adiabatic wall as N decreases from 20 to 1. Again, it interesting to note that for N=-20, the effect of solutal buoyancy force is in the opposite direction of thermal buoyancy force. Therefore, it is noticed that the magnitude of the thermal buoyancy force is very small compared to the solutal buoyancy force. For which reason we can see the streamlines are in clockwise direction which is different from other two figures of streamlines. As N decreases the isotherms are dispersed towards the adiabatic walls form the cold wall by dividing into two parts due to stronger heat transfer rate from the heated wall. But as N decreases the iso-concentrations are concentrated to the hot wall.

Fig. 5 shows the effect of N on the streamlines, isotherms and as well as on the isoconcentrations for wide range of variations in the buoyancy ratio (N) with uniformly heated and concentrated wall when $\varphi = 90^{\circ}$ and $\phi = 135^{\circ}$ for $P_r = 0.7$, $Gr_T = 10^4$, $Ha = 10^2$, $\delta = 2$, Le = 1.0 and He = 1.0. This figure shows that as buoyancy ratio decreases the streamlines are concentrated near the hot wall due the convection. When N=20 the isotherms are concentrated near the cold wall. But, as as buoyancy ratio decreases the isotherms are spreaded to the whole cavity. The iso-concentrations are mainly concentrated towards the hot wall due to the mass transfer rate at the heated wall.

Streamline, isotherm and iso-concentration contours for different values of N when P_r $0.7, Gr = 10^4, Ha = 10^2, \delta = 2, Le = 1.0, He = 1.0, \varphi = 135^{\circ} \text{ and } \phi = 45^{\circ} \text{ with uniformly}$ heated and concentrated wall are displayed in Fig. 6. Comparing Figs. 3 and 6, it can be said that the patterns of streamlines, isotherms and iso-concentrations are almost similar for uniformly heated and concentrated cases except the streamlines for value of N=-20. Here, when N = -20 the streamlines form a single eddy in the centre in anticlockwise direction.

Fig. 7 shows the effect of N on the streamlines, isotherms and as well as on the isoconcentrations for wide range of variations in the buoyancy ratio (N) with uniformly heated and concentrated wall when $\varphi = 135^{\circ}$ and $\phi = 90^{\circ}$ for $P_r = 0.7$, $Gr_T = 10^4$, $Ha = 10^2$, $\delta=2, Le=1.0, N=1.0 \text{ and } He=1.0.$ Comparing Figs. 4 and 7, it can be said that the patterns of streamlines, isotherms and iso-concentrations are almost similar for uniformly heated and concentrated cases.

Fig. 8 depicts the effect of N on the streamlines, isotherms and as well as on the isoconcentrations for wide range of variations in the buoyancy ratio (N) with uniformly heated and concentrated wall when $\varphi = 135^{\circ}$ and $\phi = 90^{\circ}$ for $P_r = 0.7$, $Gr_T = 10^4$, $Ha = 10^2$, $\delta = 2$, Le = 1.0 and He = 1.0. Comparing Figs. 5 and 8, it can be said that the patterns of streamlines, isotherms and iso-concentrations are almost similar for uniformly heated and concentrated cases.

4. Conclusion

The main objective of the current investigation is to study the effects of buoyancy ratio on an unsteady double diffusive natural convection in an inclined rectangular enclosure with different angles of magnetic field. As, the buoyancy ratio increases the boundary layer thickness

becomes thinner. The change in the flow structure for high buoyancy ratio has a significant influence on the concentration field. Formation of multiple eddies of counter-clockwise rotations greatly influences the fluid flow. When N is sufficiently small i.e, the mass buoyancy is greater than the thermal buoyancy, the buoyancy forces that drive the fluid motion are mainly due to the gradients of temperature. Negative values of N represent the opposing nature of two buoyancy forces, due to the negative coefficient of concentration expansion. In this limit, the so-called heat transfer driven flows, the distribution of constituent does not influence the flow pattern and the heat transfer rate. When N=1, the flow is steady; this is because in this case, the two buoyancies are equal to and oppose each other. When N>1, the flows driven by buoyancy due to solutal gradients where the flow are mainly due to gradients of solute concentration.

Acknowledgement Authors are thankful to the University of KwaZulu-Natal, South Africa for the support.

References

- Al-Najem, N.M., Khanafer, K.M. and El-Refaee, M.M. (1998). Numerical study of laminar natural convection in tilted enclosure with transverse magnetic field. *International Journal of Numerical Methods for Heat and Fluid Flow*, 8: 651–672.
- Chamkha, A.J. and Al-Naser, H. (2001). Double-diffusive convection in an inclined porous enclosure with opposing temperature and concentration gradients. *International Journal of Thermal Sciences*, 40: 227–244.
- Ece, M.C. and Büyük, E. (2006). Natural-convection flow under a magnetic field in an inclined rectangular enclosure heated and cooled on adjacent walls. Fluid Dynamics Research, 38: 564– 590.
- Ece, M.C. and Büyük, E. (2007). Natural convection flow under a magnetic field in an inclined square enclosure differentialy heated on adjacent walls. *Meccanica*, **42**: 435–449.
- Garandet, J.P., Alboussiere, T. and Moreau, R. (1992). Buoyancy driven convection in a rectangular enclosure with a transverse magnetic field. *International Journal of Heat and Mass Transfer*, **35**: 741–748.
- Grosan, T., Revnic, C., Pop, I. and Ingham, D.B. (2009). Magnetic field and internal heat generation effects on the free convection in a rectangular cavity filled with a porous medium. *International Journal of Heat and Mass Transfer*, **52**: 1525–1533.
- Jordan, J.Z. (2007). Network simulation method applied to radiation and viscous dissipation effects on MHD unsteady free convection over vertical porous plate. Applied Mathematical Modelling, 31: 2019–2033.
- Mahapatra, T.R., Pal, D. and Mondal, S. (2011). Natural convection in a lid-driven square cavity filled with Darcy-Forchheimer porous medium in the presence of thermal radition. *International Journal of Nonlinear Science*, 11: 366–379.
- Mahapatra, T.R., Pal, D. and Mondal, S. (2012). Influence of thermal radiation on non-Darcian natural convection in a square cavity filled with fluid saturated porous medium of uniform porosity. *Nonlinear Analysis: Modelling and Control*, 17: 223–237.
- Mahapatra, T.R., Pal, D. and Mondal, S. (2013). Effects of buoyancy ratio on double-diffusive natural convection in a lid-driven cavity. *International Journal of Heat and Mass Transfer*, **57**: 771–785.
- Mahapatra, T.R., Pal, D. and Mondal, S. (2013). Mixed convection flow in an inclined enclosure under magnetic field with thermal radiation and heat generation. *International Communications in Heat and Mass Transfer*, **41**: 47–56.
- Mansour, M.A., Chamkha, A.J., Grecos, R.A., Abd El-Aziz, M.M. and Ahmed, S.E. (2010). MHD natural convection in an inclined cavity filled with a fluid saturated porous medium with heat source in the solid phase. *Nonlinear Analysis: Modelling and Control*, 15: 55–70.
- Mondal, S. and Sibanda, P. (2015). Effects of buoyancy ratio on unsteady double-diffusive natu-

- ral convection in a cavity filled with porous medium with non-uniform boundary conditions. International Journal of Heat and Mass Transfer, 85: 401–413.
- Moufekkir, F., Moussaoui, M.A., Mezrhab, A., Bouzidi, M. and Laraqi, N. (2013). Study of doublediffusive natural convection and radiation in an inclined cavity using lattice Boltzmann method. International Journal of Thermal Sciences, 63: 65–86.
- Rahman, R. and Sharif, M.A. (2003). Numerical study of laminar natural convection in inclined rectangular enclosures of various aspect ratios. Numerical Heat Transfer Part A, 44: 355-373.
- Rudraiah, N., Barron, R.M., Venkatachalappa, M. and Subbaraya, C.K. (1985). Effect of magnetic field on free convection in a rectangular enclosur. International Journal of Engineering Science, **33**: 1075–1084.
- Sarris, I.E., Kakarantzas, S.C., Grecos, A.P. and Vlachos, N.S. (2005). MHD natural convection in a laterally and volumetrically heated square cavity. International Journal of Heat and Mass Transfer, 48: 3443-3453.
- Shercliff, J. A. (1965). A Textbook on Magnetohydrodynamics, Pergamon Press, Oxford.
- Teamah, M.A., Elsafty, A.F., Elfeky, M.Z. and El-Gazzar, E.Z. (2011). Numerical simulation of double-diffusive natural convective flow in an inclined rectangular enclosure in the presence of magnetic field and heat source, part A: Effect of Rayleigh number and inclination angle. Alexandria Engineering Journal, 50: 269–282.
- Teamah, M.A., Sorour, M.M., El-Maghlany, W.M. and Afifi, A. (2013). Numerical simulation of double diffusive laminar mixed convection in shallow inclined cavities with moving lid. Alexandria Engineering Journal, 52: 227–239.
- Wang, G., Wang, Q., Zeng, M. and Qzoe, H. (2008). Numerical study of natural convection heat transfer in an inclined porous cavity with time-periodic boundary conditions Transport in Porous Media, 74: 393-409.

Table 1. Grid independence test when $P_r = 0.7$, $Gr = 10^4$, $Ha = 10^2$, $\delta = 2$, Le = 1.0, He = 1.0, $\varphi = 45^\circ$, $\phi = 45^{\circ}$ and N = 1.

Grid points	Iter	$ \psi_{ ext{max}} $
20×20	34368	5.95110×10^{-2}
40×40	131880	6.00418×10^{-2}
80×80	530782	6.01884×10^{-2}
160×160	1162672	6.01887×10^{-2}

Table 2. Comparison of average Nusselt number $\overline{Nu}_H|_{x=0}$ in absence of concentration equation, thermal radiation parameter and heat generation parameter with same boundary conditions and same values of all other parameters.

	$\overline{Nu_H}$								
	$\varphi = 0^{\circ}$			$\varphi = 45^{\circ}$			$\varphi = 90^{\circ}$		
φ	Mahapatra et al., (2013)		Present Results			Present Results			Present Results
00	3.5350	3.6831	3.5350	3.5354	3.6819	3.5354	3.5356	3.6813	3.5356
-45	3.5363	3.6806	3.5363	3.5366	3.6846	3.5366	3.5363	3.6843	3.5363
45°	3.5340	3.6780	3.5340	3.5339	3.6820	3.5339	3.5341	3.6806	3.5341

Table 3. Computed values of \overline{Nu}_H and \overline{Sh}_H when $P_r=0.7,~Gr=10^4,~Ha=10^2,~\delta=2,~Le=1.0$ and He=1.0 for various values of $\varphi,~\phi$ and N.

		Buoyan	cy ratio	Buoya	ncy ratio	Buoyancy ratio		
		N=20		N = 1		N = -20		
φ	ϕ	\overline{Nu}_H	\overline{Sh}_H	\overline{Nu}_H	\overline{Sh}_H	\overline{Nu}_H	\overline{Sh}_H	
	45°	1.94699	8.93750	1.67498	7.50946	1.88540	7.85743	
45°	90°	2.11064	7.93526	1.68330	7.5132655	1.76858	7.57010	
	135°	2.42024	8.52446	1.68626	7.51558	2.44834	8.40416	
	45°	2.65610	10.73437	1.67736	7.51126	2.19201	8.56903	
90°	90°	2.66738	9.10950	1.70193	7.52637	1.88740	7.73783	
	135°	3.00922	11.00129	1.71378	7.54384	3.00949	10.23665	
	45°	1.931679	8.37004	1.67510	7.50954	1.86995	7.96886	
135°	90°	2.12979	7.80844	1.68421	7.51211	1.84856	7.613725	
	135°	2.46780	8.76437	1.68908	7.51589	2.42373	8.37702	

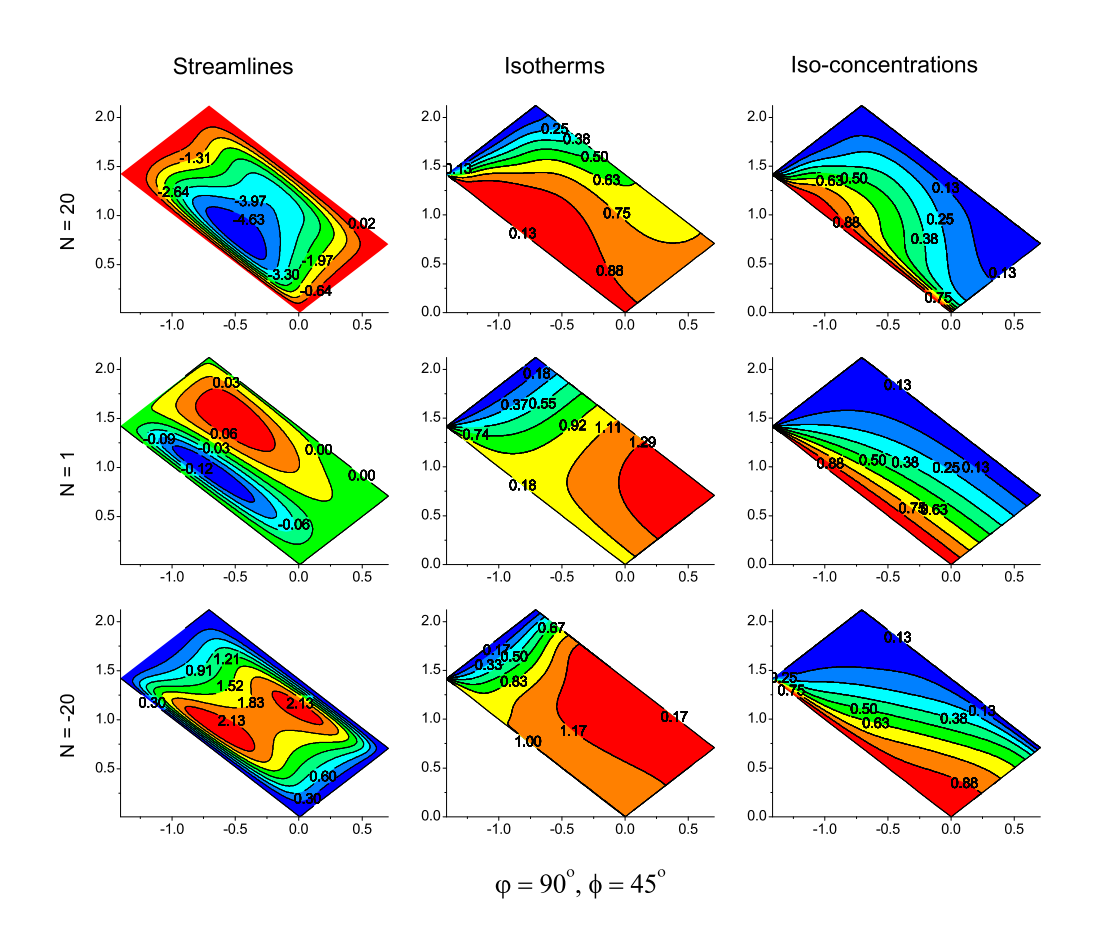


Fig. 3. Contour plots for $P_r=0.7$, $Gr=10^4$, $Ha=10^2$, $\delta=2$, Le=1.0, He=1.0, $\varphi=90^\circ$, $\phi=45^\circ$ for different values of N.

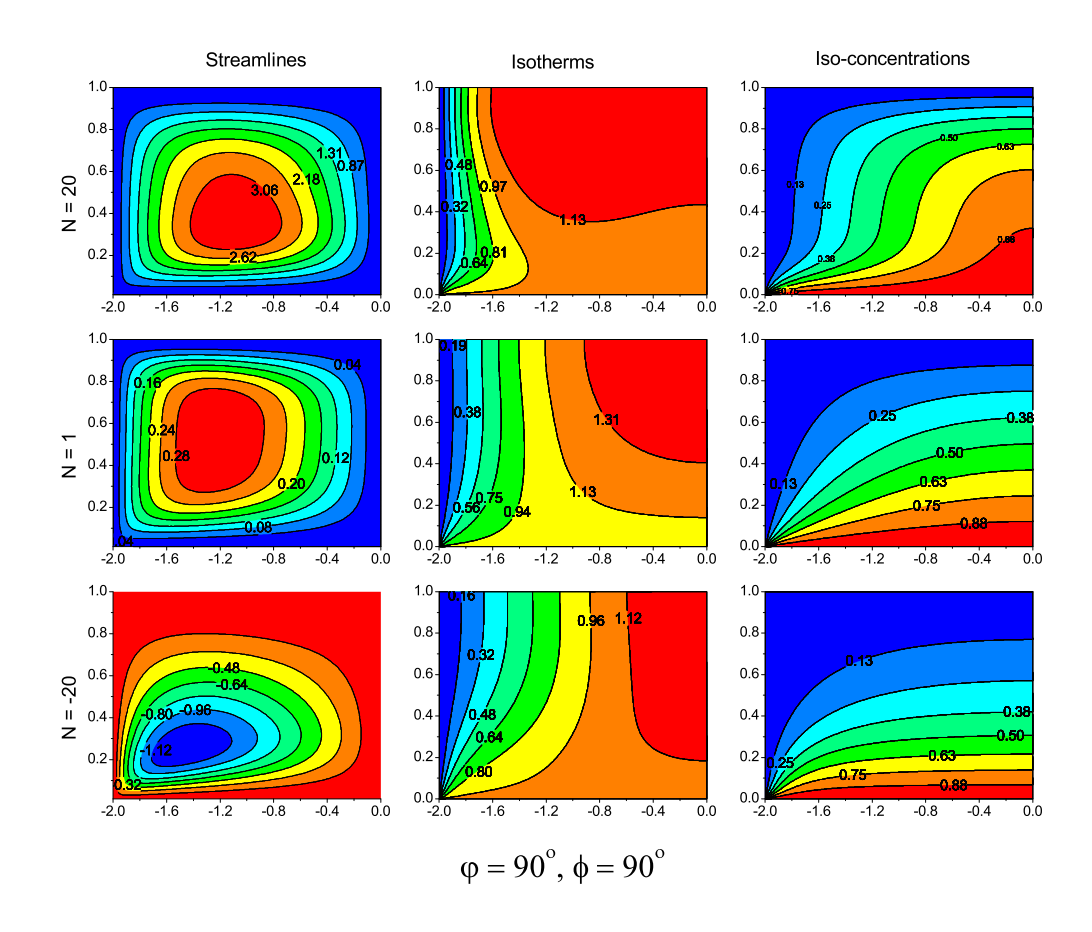


Fig. 4. Contour plots for $P_r = 0.7$, $Gr = 10^4$, $Ha = 10^2$, $\delta = 2$, Le = 1.0, He = 1.0, $\varphi = 90^\circ$, $\phi = 90^\circ$ for different values of N.

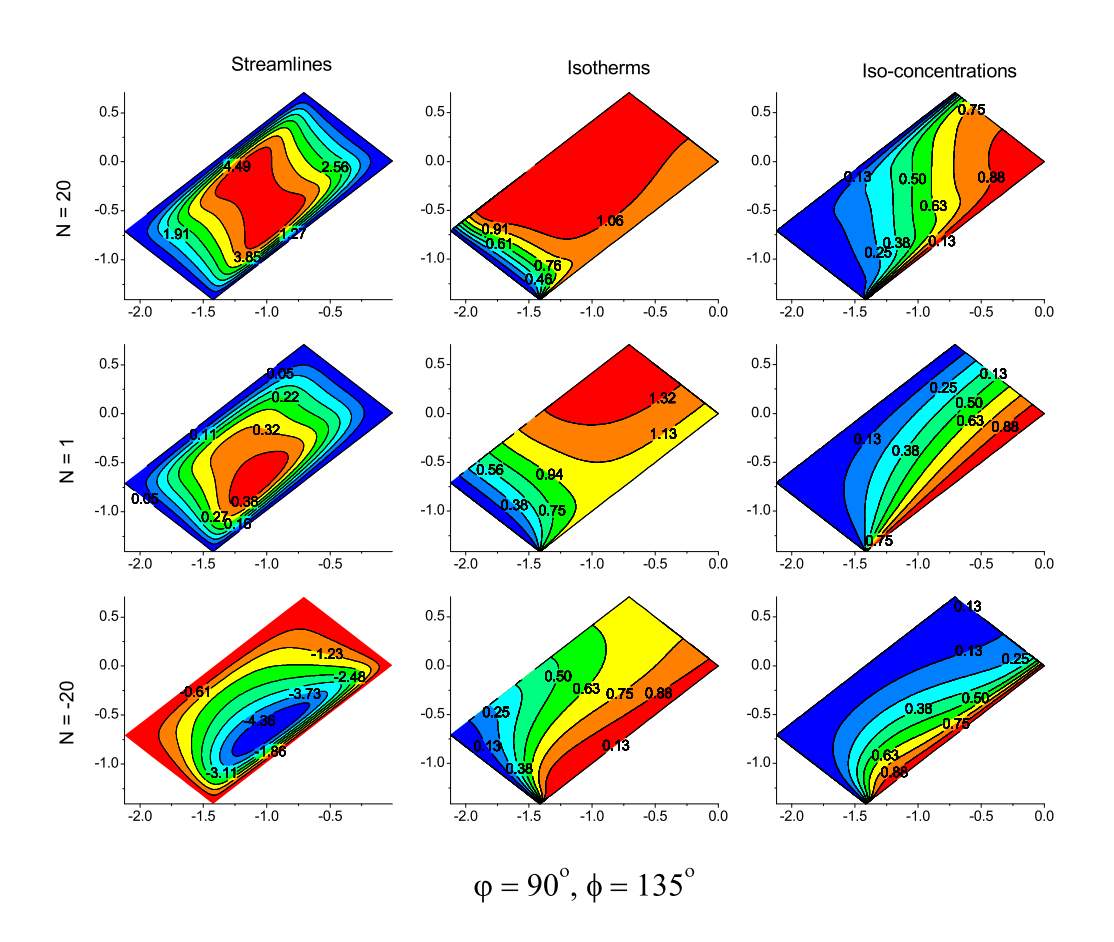


Fig. 5. Contour plots for $P_r=0.7,~Gr=10^4,~Ha=10^2,~\delta=2,~Le=1.0,~He=1.0,~\varphi=90^\circ,~\phi=135^\circ$ for different values of N.

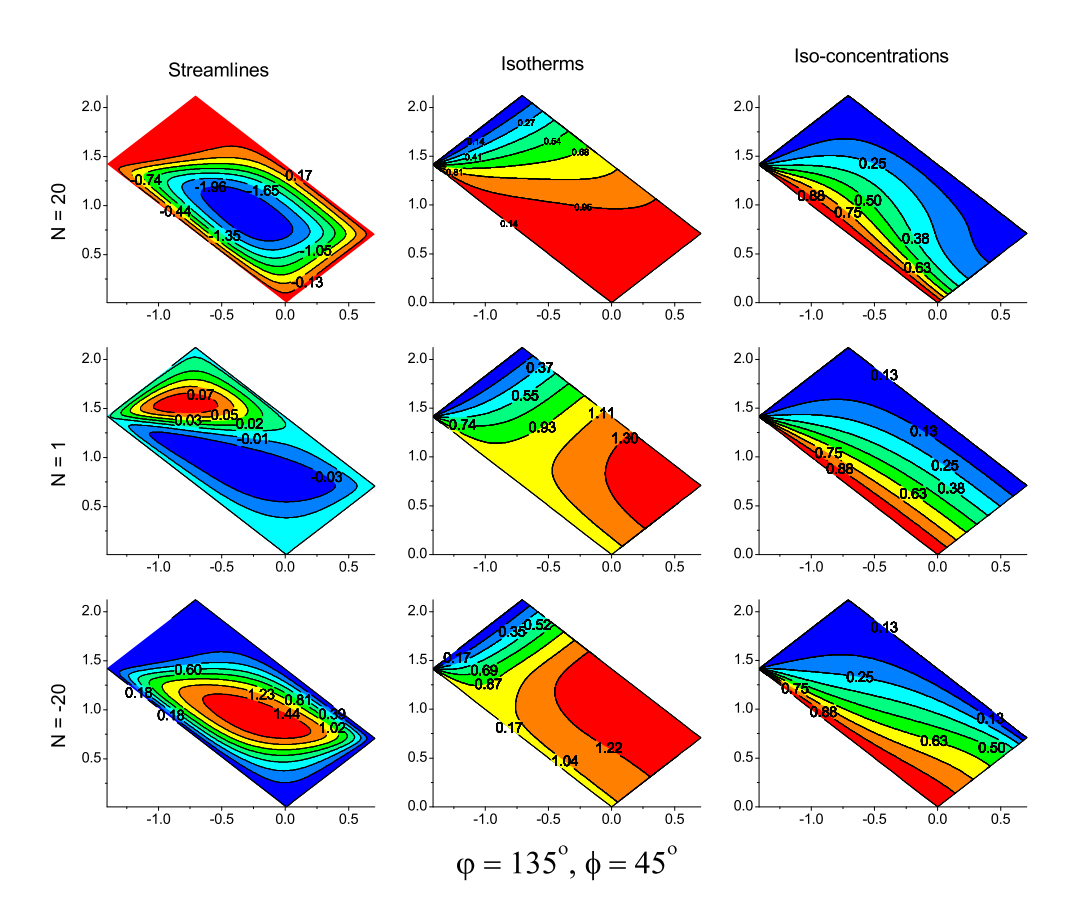


Fig. 6. Contour plots for $P_r = 0.7$, $Gr = 10^4$, $Ha = 10^2$, $\delta = 2$, Le = 1.0, He = 1.0, $\varphi = 135^\circ$, $\phi = 45^\circ$ for different values of N.

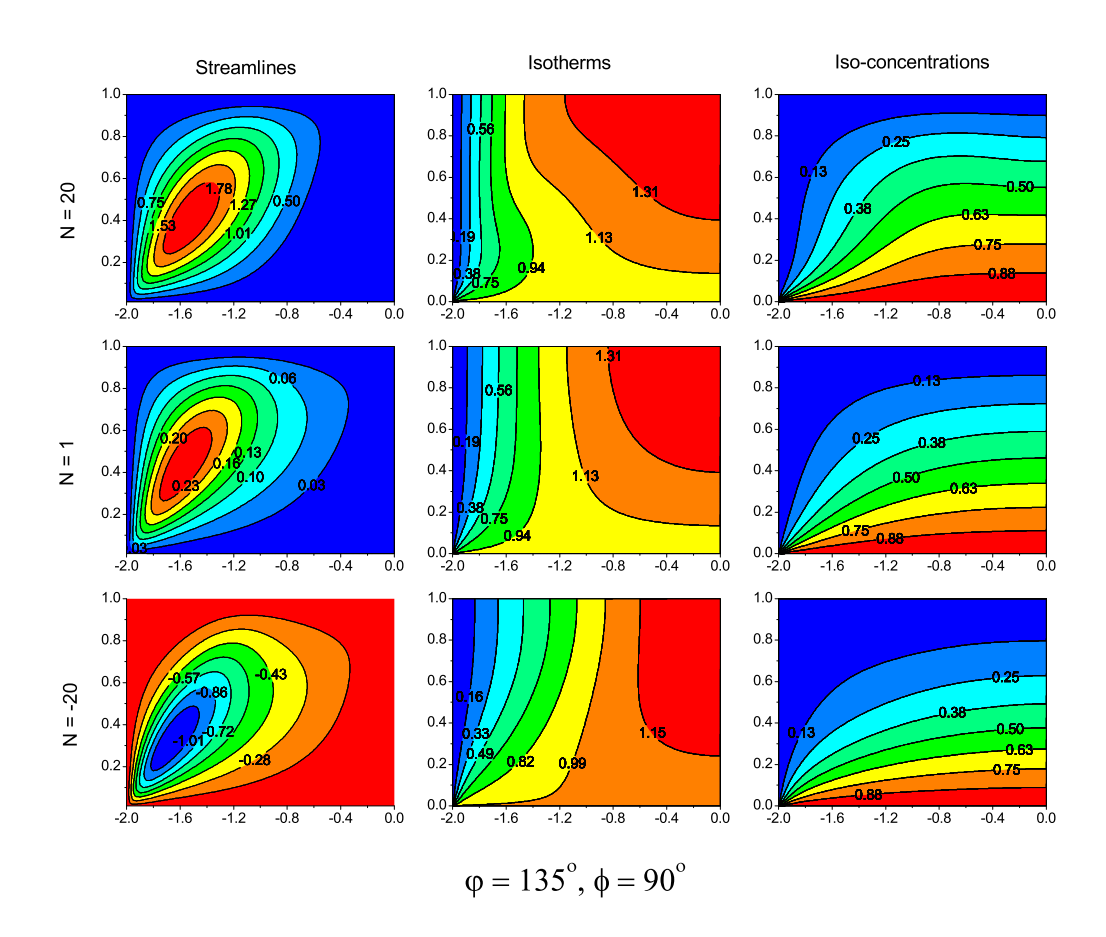


Fig. 7. Contour plots for $P_r=0.7$, $Gr=10^4$, $Ha=10^2$, $\delta=2$, Le=1.0, He=1.0, $\varphi=135^\circ$, $\phi=90^\circ$ for different values of N.

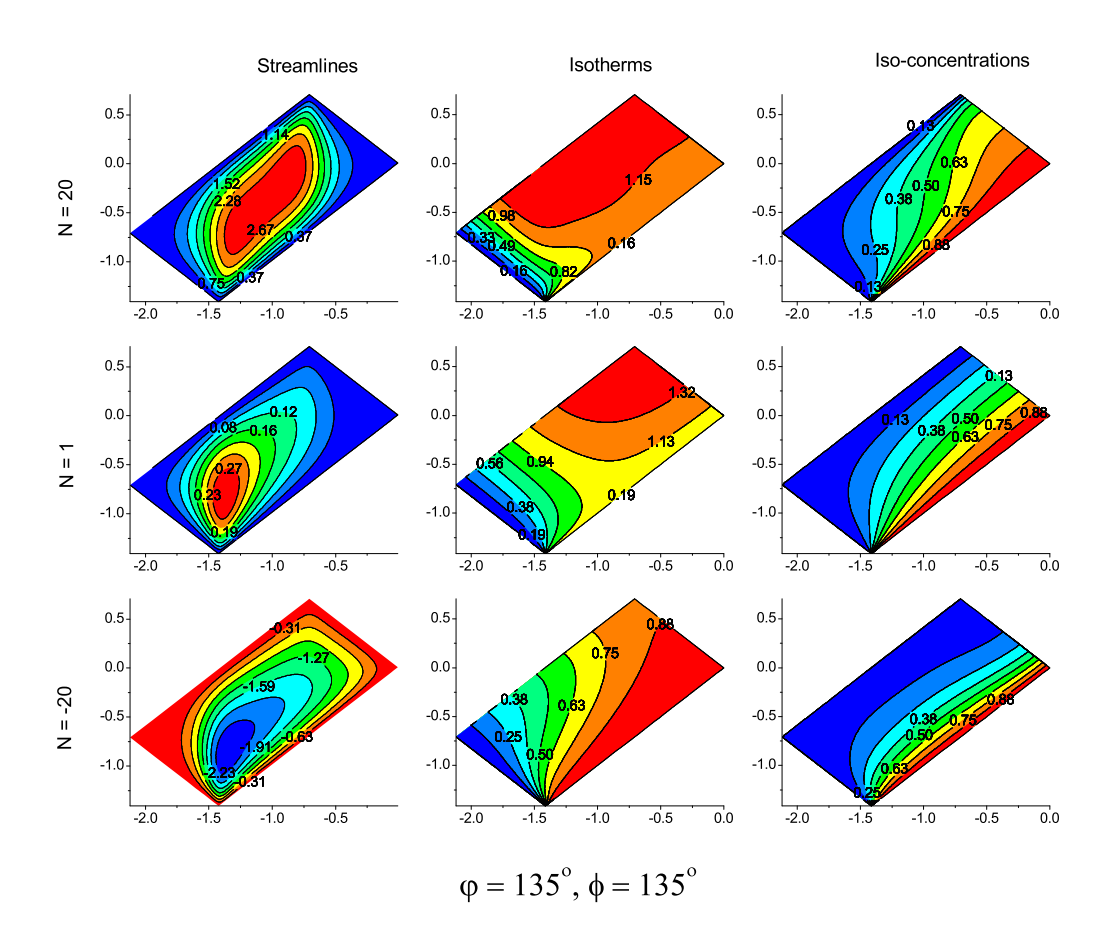


Fig. 8. Contour plots for $P_r = 0.7$, $Gr = 10^4$, $Ha = 10^2$, $\delta = 2$, Le = 1.0, He = 1.0, $\varphi = 135^\circ$, $\phi = 135^\circ$ for different values of N.